Superradiance and Exciton Delocalization in Perovskite Quantum Dot Superlattices

Daria D. Blach,[1#] Victoria A. Lumsargis,[1#] Daniel E. Clark, [1#] Chern Chuang,[2] Kang Wang,[3] Letian Dou,[3] Richard D. Schaller,[4,5] Jianshu Cao,[6] Christina W. Li,[1]* and Libai Huang[1]*

[1] Department of Chemistry, Purdue University, West Lafayette, Indiana 47907, United States

[2] Department of Chemistry, University of Toronto, Toronto, Ontario M5S1A4, Canada

[3] Davidson School of Chemical Engineering, Purdue University, West Lafayette, Indiana 47907, United States

[4] Department of Chemistry, Northwestern University, Evanston, Illinois 60208, United States

[5] Center for Nanoscale Materials, Argonne National Laboratory, Lemont, Illinois 60439, United States

[6] Department of Chemistry, Massachusetts Institute of Technology, Cambridge, Massachusetts 02139, United States

#These authors contributed equally.

*Corresponding authors: libai-huang@purdue.edu; christinawli@purdue.edu

Abstract

Achieving superradiance in the solid-state is challenging due to fast dephasing processes from inherent disorder and thermal fluctuations. Perovskite quantum dots (QDs) are an exciting class of exciton emitters with large oscillator strength and high quantum efficiency, promising for solid-state superradiance. However, a thorough understanding of the competition between coherence and dephasing from phonon scattering and energetic disorder is currently unavailable. Here, we present an investigation of exciton coherence in perovskite QD solids using temperature-dependent photoluminescence linewidth and lifetime measurements. Our results demonstrate that excitons are coherently delocalized over 3 QDs at 11 K in superlattices leading to superradiant emission. Scattering from optical phonons leads to the loss of coherence and exciton localization to a single QD at temperatures above 100 K. At low temperatures, static disorder and defects limit exciton coherence. These results highlight the promise and challenge in achieving coherence in perovskite QD solids.

Keywords: Quantum dot solids, superradiance, exciton coherence, perovskite

The realization of robust coherence in the solid-state has been a long-standing challenge for quantum materials research. Superradiance, proposed by Dicke in 1954, describes a macroscopically coherent state that arises from the excitation of an ensemble of individual dipole emitters,[1] which is characterized by an accelerated radiative decay rate proportional to the number of emitters *N*. Realization of superradiance solid-state systems is challenging due to inherent inhomogeneities and unavoidable fast dephasing processes.[2-4] Recently, colloidal metal halide perovskite quantum dots (QDs) have emerged as an exciting class of quantum emitters due to their near-unity quantum yields, large oscillator strengths, and long coherence time.[5-13] Superfluorescence, a many-body superradiance in which the transition dipole of many QDs self-lock into a macroscopic dipole after being photoexcited, has been recently reported in self-assembled perovskite QD superlattices (SLs).[14, 15]

When inter-QD electronic coupling is larger than other dephasing fluctuations, a symmetric delocalized state is produced by the quantum superposition of all *N* possible single QD excitations. This delocalized state is superradiant because the transition dipole moment is enhanced by a factor of *N*, which is known as single-photon superradiance.[16] Here, accelerated decay can be observed even if only one QD is excited. Such superradiance has been demonstrated in molecular aggregates with excitons delocalized over hundreds of molecules at low temperatures due to their strong electronic coupling (up to 200 meV).[17-22] Currently, a thorough understanding of the interplay between disorder and coherence in perovskite QD solids is lacking; such understanding is crucial for harnessing superradiance resulting from exciton delocalization to boost the performance of optoelectronic devices and engineer new quantum light sources. To address this question, we employed temperature-dependent and time-resolved photoluminescence (PL) spectroscopy to quantify exciton delocalization. We show that dipole coupling can outcompete disorder at low

temperatures, resulting in single-photon superradiant radiative decay with a coherence number around 3 at 11 K for highly ordered SLs.

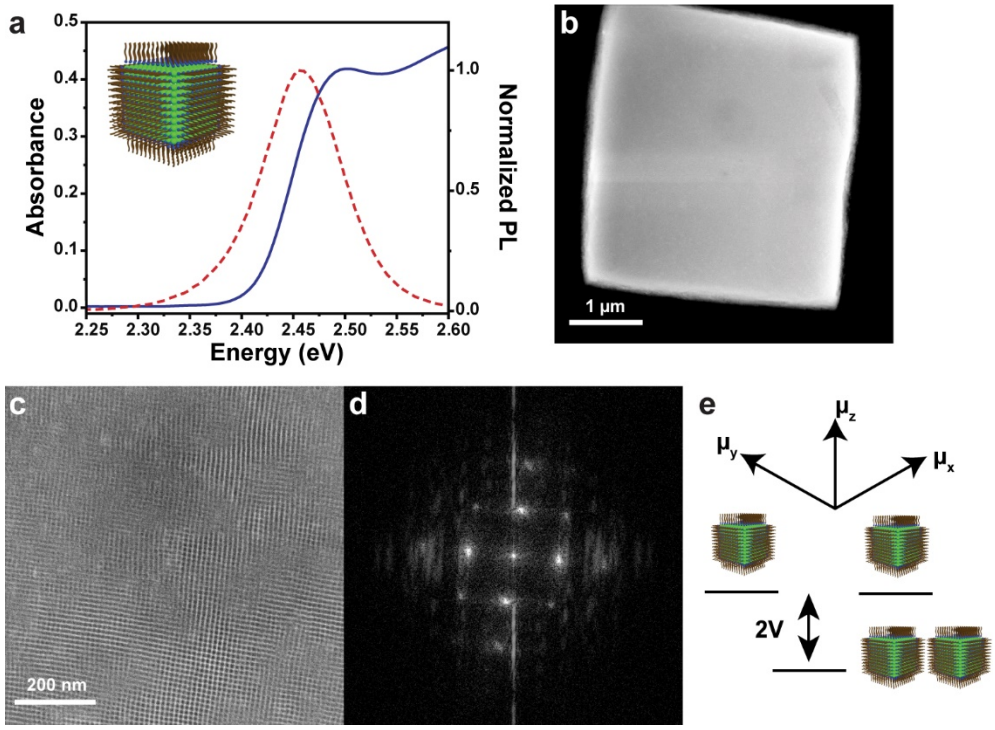

Fig. 1. Structural and optical characterization of the $CsPbBr_3$ QD SLs. (a) Absorbance and PL spectra of $CsPbBr_3$ QDs in toluene. Inset: schematic illustration of a $CsPbBr_3$ QD capped with oleylamine and oleic acid. (b) Low-resolution HAADF-STEM image of a single SL. (c) High-resolution HAADF-STEM image of the same SL taken in the center showing ordered QD packing. (d) FFT of the high-resolution image. (e) Schematic of the nearest-neighbor dipole coupling between excitons in a QD dimer.

We employed highly ordered QD SLs with a small size distribution and well-defined inter-QD distance to probe the interplay between coherence and dephasing. Colloidal $CsPbBr_3$ QDs, whose absorbance and PL spectra are shown in Fig. 1a (Fig. S1 includes QD size distribution), were assembled into close-packed, three-dimensional (3D) micron-sized SLs on a silica substrate through slow evaporation (Fig. S2).[23] To examine the ordering, high-angle annular dark-field scanning transmission electron microscopy (HAADF-STEM) images were collected on two representative SLs (Fig. 1b-c and Fig. S3a-b). Cubic packing of QDs within the SL can be observed (Fig. 1c). Fast-Fourier transforms (FFT) of STEM images indicate long-range order within a given

SL (Fig. 1d and Fig. S3c). For the SL shown in Fig. 1b-c, a well-defined spacing between the QDs (r) is apparent. The first set of reflections occurs at 12 nm/c, a spacing that closely corresponds to the length of a 9 nm QD combined with a 3 nm spacing due to capping ligands.[23] In contrast, the SL shown in Fig. S3a exhibits much greater disorder in the FFT as depicted in Fig. S3c. A broad smear is observed from 10-14 nm/c, indicating substantial heterogeneity of r for the QD packing in this SL.

Electronic Coupling. Fig. 1e illustrates the electronic coupling between excitons in $CsPbBr_3$ QDs due to dipole-dipole interaction. This static dipole interaction is valid for distances smaller than the emission wavelength. Radiative coupling, which is important at distances longer than the emission wavelength,[24] is neglected here and merits further investigation. For an isolated $CsPbBr_3$ QD, the lowest exciton state is a bright triplet with transition dipoles oriented in the x, y, and z directions.[12] The nearest-neighbor dipole-dipole coupling is given by

$$V = \frac{\kappa \mu^2}{\varepsilon R^3} \quad (1)$$

where μ is the transition dipole, κ is the orientation factor, ε is the dielectric constant, and R is the inter-QD distance. In dimers, the lowest state lies $2V$ below the isolated QD transition.[25] In 3D SLs, exciton bands form due to periodic boundary conditions.[26] The lowest energy state at $k = 0$ (zero momentum, Brillouin zone center) is superradiant, which is the quantum superposition of all N possible single QD excitations. However, disorder can localize excitons by randomizing the relative frequency and phases. This scatters the population from the delocalized $k = 0$ state to localized states with finite momentum, which leads to the destruction of coherence.[19]

We carried out PL and reflectance spectroscopy over a wide temperature range (11-295 K) on multiple SLs grown on five different substrates, denoted as A, B, C, D, and E (Fig. S4), to evaluate the degree of electronic coupling and disorder. Results from these SLs were compared to

a thin film of highly dispersed QDs in a polymethyl methacrylate (PMMA) matrix, with mostly isolated QDs and small clusters (Fig. S5a). The PL spectra for isolated QDs and the A1 SL are shown in Figs. 2a and 2b, respectively (data for other SLs is shown in Fig. S6). The center peak position and linewidth are compared for the isolated QDs and the A1 SL in Fig. 2c-d (other SLs presented in Fig. S7). For the isolated QDs, the PL and reflectance (Fig. S8) peak position red-shifts slightly as temperature decreases, which is mainly attributed to the reduced bandgap due to the decreased lattice constant at low temperatures.[27] While the center peak position for A1 and isolated QDs is similar between 100-295 K, the peak center of the SL further red-shifted from the isolated QDs below 100 K, with a shift of ~19 meV at 11 K.

The red-shifted and narrower PL emission for the SLs at low temperatures is an optical signature of superradiance, where the collective excitonic states are shared by more than one QD. The energy shift is proportional to the effective dipole coupling strength V.[28] As detailed in the SI, we estimated V to be ~16 meV, which is on the same order as the observed PL peak shift at 11 K and an order of magnitude higher than CdSe QD SLs.[29] Temperature-dependent reflectance spectra further confirm that red-shifted PL emission originated from the delocalized superradiant state. For the SL, we observed red-shifted exciton resonance with increased oscillator strength at low temperatures, consistent with superradiance (Fig. 2e). In contrast, for isolated QDs, exciton absorption does not change significantly as a function of temperature (Fig. S8). In addition, the energy gap between absorption and PL peak is constant across all temperatures in the SLs (Fig. 2f), which validates that the red-shifted emission at low temperatures does not result from other effects such as energy transfer from smaller to larger QDs. The larger red-shift at lower temperatures can be explained by how the transition dipole in isolated QDs increases due to the exciton size increasing.[30, 31] Although the A, C, D, and E SLs examined here have different sizes

and shapes (Fig. S4), they have qualitatively similar behaviors. Therefore, we conclude that photonic effects do not play an important role here.

Phonon Scattering. For both the SLs and isolated QDs, the PL linewidth becomes narrower at lower temperatures, consistent with the reduced dynamic disorder from phonon scattering.[32] From Fig. 2d, we observe that for isolated QDs, the linewidth becomes constant below 100 K. In contrast, for some SLs, the linewidth continues to narrow below 100 K (data for A1 SL shown in Fig. 2d, other SLs in Fig. S7). This can be explained by exchange narrowing, where narrower linewidths result from the averaging of inhomogeneities over many QD sites due to excitation delocalization at low temperatures.[20] Thus, the additional narrowing of the PL linewidth at low temperatures also confirms that excitons are delocalized over multiple QDs at low temperatures in some SLs.

Both acoustic and optical phonon scattering could contribute to the linewidth. We extracted the phonon scattering strength by fitting the temperature-dependent PL linewidth

$$FWHM = \Gamma_0 + \Gamma_{AC}T + \frac{\Gamma_{LO}}{e^{\frac{E_{LO}}{k_B T}} - 1} \quad (2)$$

where Γ_0 is the inhomogeneous linewidth due to static disorder, Γ_{AC} (Γ_{LO}) is the exciton-longitudinal acoustic (optical) phonon coupling strength, E_{LO} is the energy of optical phonons, k_B is the Boltzmann distribution, and T is temperature.[33-36] We fixed E_{LO} to 16 meV corresponding to Pb-Br bending motions based on a previous work.[37] Fitting parameters are listed in Table S1. The Γ_{LO} values are similar for all SLs (~40 meV), indicating similar electron-phonon coupling strength. Overall, the coupling of optical phonons dominates the temperature-dependent linewidth, and the contribution from acoustic phonons is negligible, consistent with previous reports.[38]

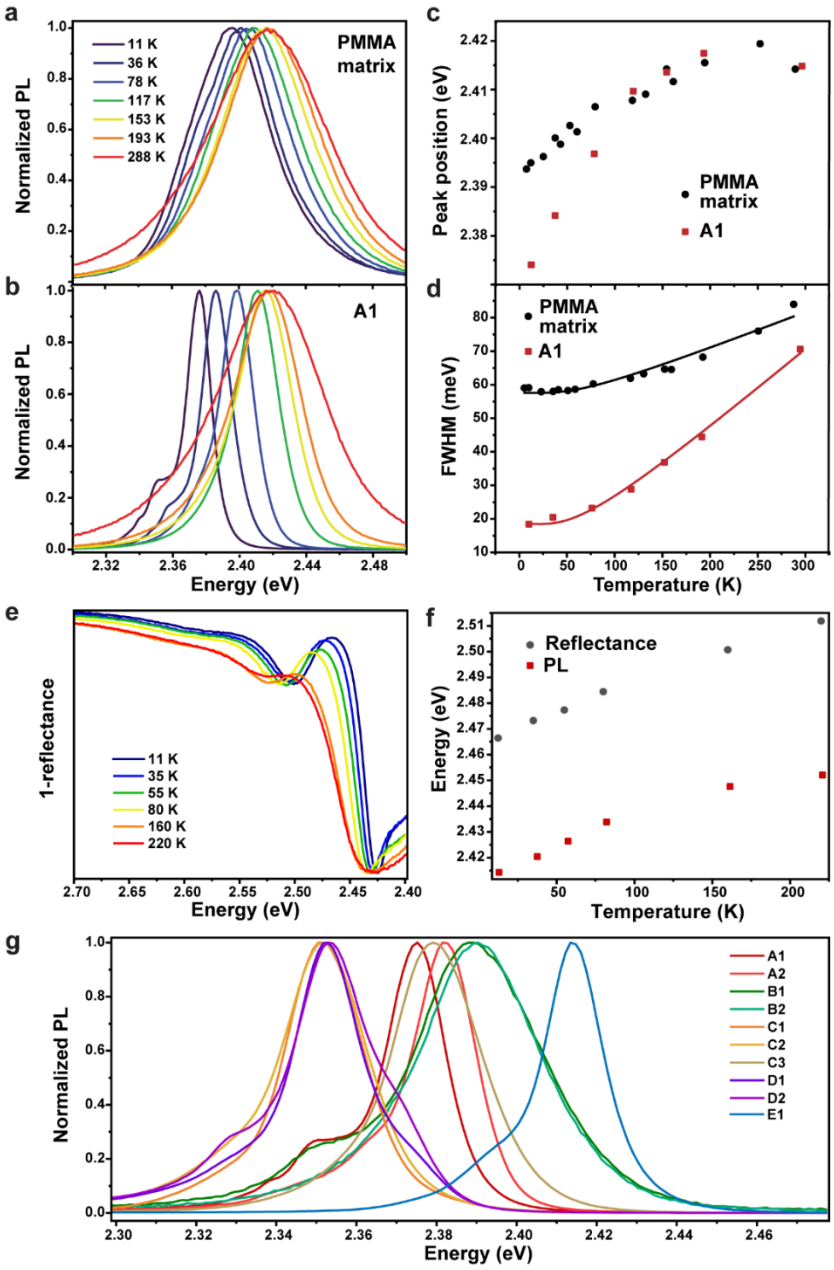

Fig. 2. Temperature-dependent PL and reflectance spectroscopy to elucidate dynamic and static disorder. Temperature-dependent PL spectra acquired between 11 K and 295 K for (a) isolated QDs and (b) the A1 SL. (c) Temperature-dependent center peak position extracted from PL spectra of isolated QDs and A1 SL. (d) Temperature-dependent FWHM extracted from PL spectra of isolated QDs and A1 SL. (e) Reflectance spectra for E1 SL collected at temperatures between 11 K and 220 K. (f) Temperature-dependent energy shift for reflectance and PL shown for E1 SL. (g) PL spectra of all SLs collected at 11 K.

Static Disorder. We use Γ_0 as a measure of static disorder from inhomogeneities and Fig. 2g compares the PL spectra at 11 K. Static disorder has two main contributions: the size

distribution of individual QDs that leads to different exciton energies and the inhomogeneities in the inter-QD distance resulting in fluctuations of QD-to-QD coupling. As shown in Fig. 2g, all SLs have a narrower linewidth (17-35 meV) compared to isolated QDs (60 meV). The narrower linewidth indicates SLs have smaller static disorder, as expected from the selection of a subpopulation of QDs with a smaller size distribution than the overall population through self-assembly. There are also variations in the PL linewidth between SLs, even when grown on the same substrate (e.g. C1, C2, and C3). A1 and E1 have the smallest FWHM (~18 meV), and B1 has the broadest (35 meV). Further examination of the PL spectra at 11 K in Fig. 2g shows that some SLs have lower-energy shoulder peaks. These are most likely caused by the existence of subdomains, composed of different sizes of QDs, within individual SLs.[14, 39]

Superradiance Enhanced Radiative Rate. The red-shifted and narrower PL emission of the SLs compared to isolated QDs at low temperature indicates that the exciton coherence length could extend beyond one QD. To determine which SLs support superradiance, we compare the temperature-dependent PL decay of isolated QDs and the A1 SL in Figs. 3a and 3b, respectively (Fig. S9 includes other SLs' PL lifetimes). The averaged PL lifetime was determined by taking the 1/e value of the obtained dynamics curve. While the low-energy shoulder corresponding to subdomains with larger QDs could have slightly slower decay, energy transfer from smaller to larger QDs does not affect the extracted PL lifetime significantly (Fig. S10), which could be explained by the radiative decay being faster or comparable to the energy transfer time.[40] As the PL decay contains contributions from both radiative and non-radiative decay pathways, temperature-dependent PL quantum yields (PLQYs) were calculated, as shown in Fig. 3c (calculation details are provided in the SI). The 1/e lifetimes and PLQYs were used to calculate the radiative rates. For isolated QDs, the absolute PLQY at 295 K was measured to be 92 ± 5%.

The PLQYs at different temperatures and in the SLs were determined relatively after correcting for temperature-dependent absorption.[41] The relative PLQY of the isolated QDs and A1 SL are shown in Fig. 3c (other SLs' PLQYs are included in Fig. S11). The calculated temperature-dependent radiative rate for the isolated QDs and A1 SL are compared in Fig. 3d (other SLs are shown in Fig. S12). The uncertainties in the PLQYs and, consequently, radiative rates are largely due to heterogeneity (demonstrated in a PL intensity map of a representative SL in Fig. S13). At room temperature, the PLQY values vary from SL to SL and are consistently lower than that of the isolated QDs, likely due the increased probability of non-radiative energy transfer to defect sites in the SLs.[42, 43] At low temperatures, the radiative rate in highly ordered SLs is enhanced by superradiance, which can outcompete non-radiative pathways and lead to PLQY close to 1.

Overall, the radiative rate increases as temperature decreases, as shown in Fig. 3d for the A1 SL and isolated QDs (other SLs included in Fig. S12). Below 100 K, the radiative lifetime in the A1 SL becomes significantly shorter than the isolated QDs. At 11 K, the radiative rate in the A1 SL is 3.2 ns^{-1}, compared to 1.2 ns^{-1} for the isolated QDs, which implies that the coherence length extends beyond one QD. In other words, superradiance is achieved when the transition dipole moment from multiple QDs merge into a single, large dipole (i.e. $N>1$). We determined the average N by taking the ratio of the SL and isolated QD's radiative rates. On average, 3 QDs are coherently coupled at 11 K in the A1 SL. We note that the radiative rate for the isolated QDs also increases from 0.4 ns^{-1} to 1.2 ns^{-1} as the temperature decreases from 298 K to 11 K (Fig. 3d). The enhanced radiative rate of isolated QDs at low temperatures can be explained by the increased exciton size, as phonon scattering is reduced.[30, 31]

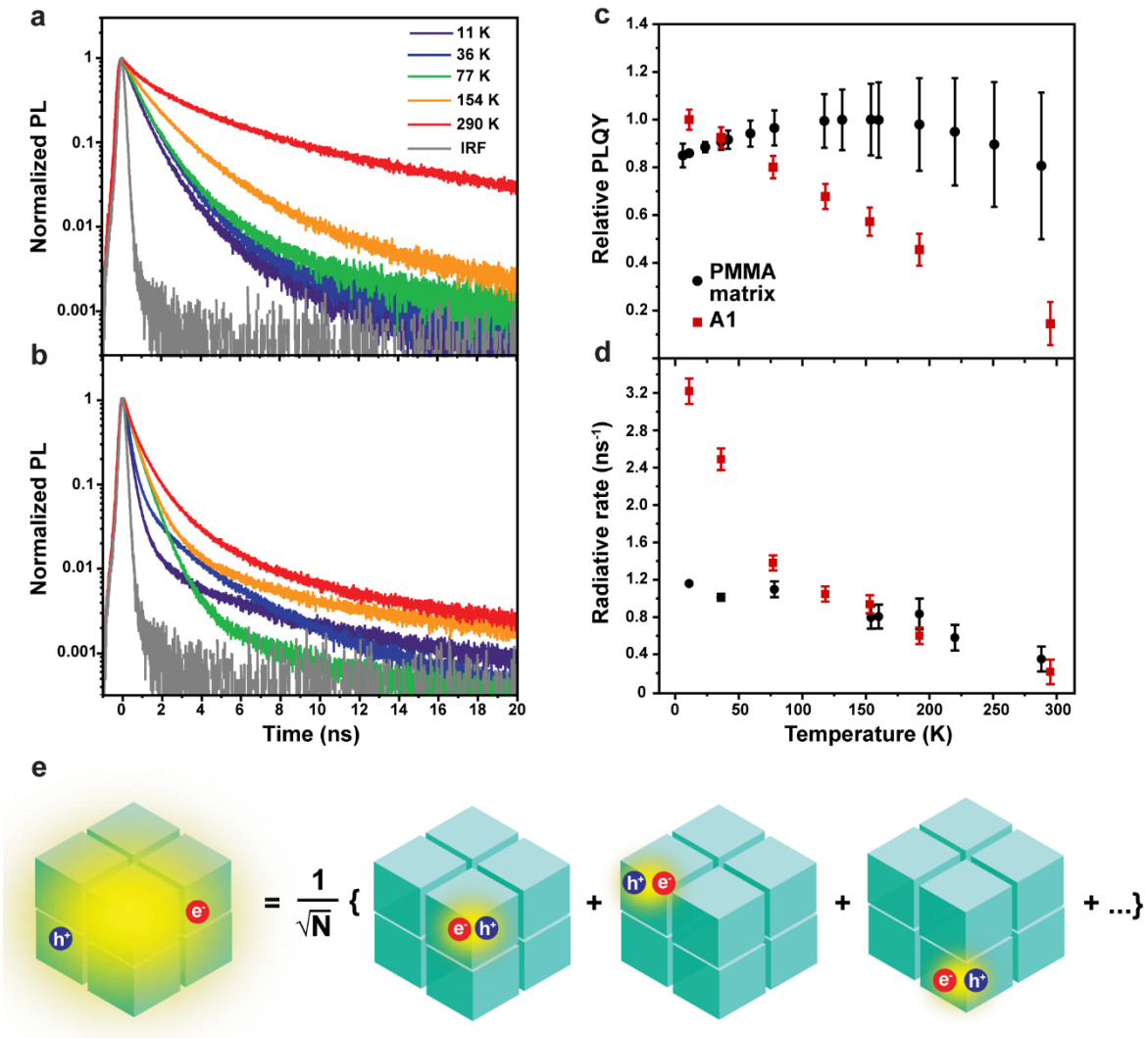

Fig. 3. Superradiance enhanced radiative rates in SLs. Temperature-dependent PL lifetimes of (a) isolated QDs and (b) coupled QDs in A1 SL. (c) Temperature-dependent relative PLQY for isolated QDs and A1 SL. (d) Temperature-dependent radiative rates for isolated QDs and A1 SL. (e) Schematic illustration of the superradiant state produced by the quantum superposition of all *N* possible single QD excitations. *N=3* for the A1 SL.

The superradiance observed here is different from previously reported superfluorescence.[13, 14] For superfluorescence, many QDs are excited and a burst of intense emission appears only above certain pump intensity thresholds after a time delay due to the time necessary for dipoles to become aligned by an external field.[2] *N* is dependent on how many QDs are excited and is varied with pump intensity. Here, the accelerated PL decay occurs at zero delay (also confirmed with a higher temporal resolution of ~25 ps, Fig. S14) and is independent of pump

intensity (Fig. S15). We attribute this to single-photon superradiance,[16] where the quantum superposition of N single emitter excitations produces a symmetric superradiant state (schematically shown in Fig. 3e). Such superradiance occurs even when the system interacts with one photon, therefore, all but one of the QDs are in the ground state, which is similar to the superradiance observed in molecular J-aggregates. At high pump intensities, PL decay could become shorter due to exciton-exciton annihilation.[44]

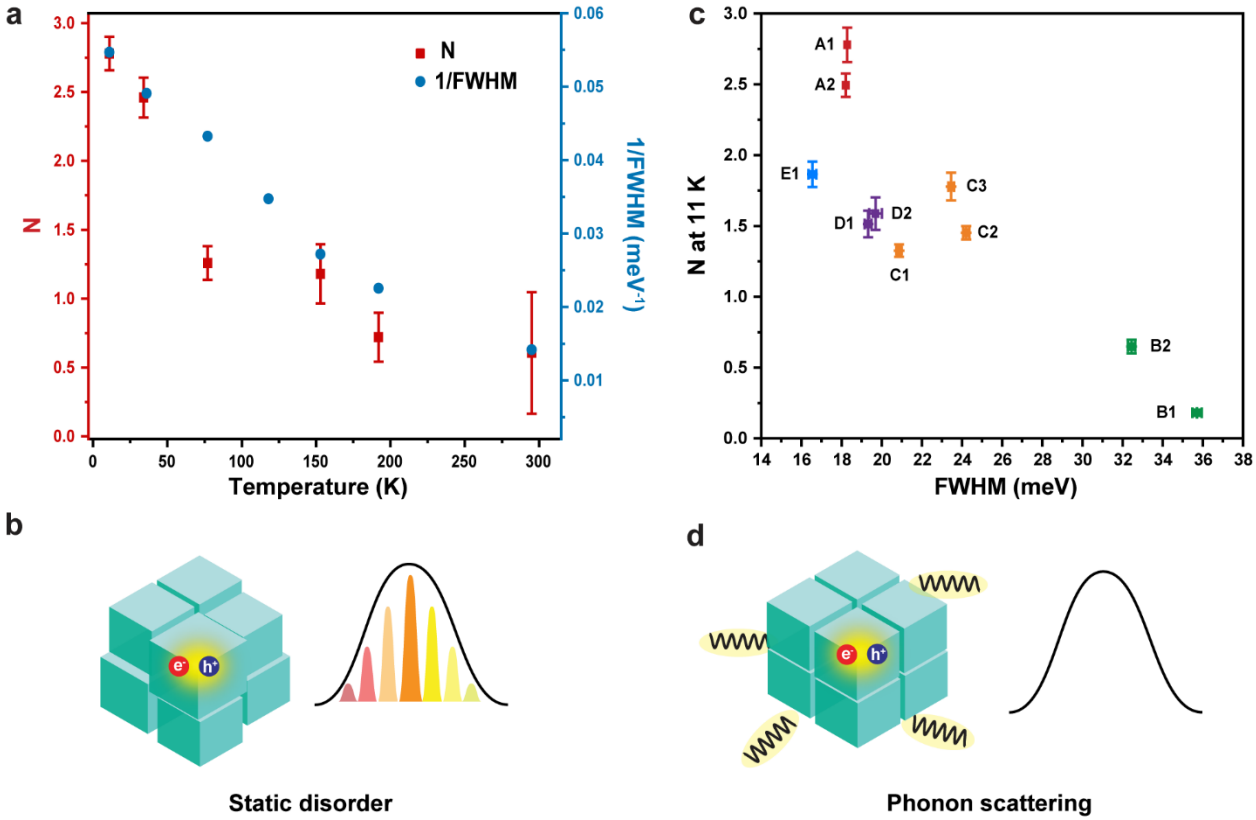

Fig. 4. Phonon and disorder limited exciton superradiance. (a) The temperature dependence on N and the inverse of the FWHM for the A1 SL. (b) Diagram showing exciton localization due to phonon scattering at high temperatures. (c) Comparison of each SLs' N plotted against their respective FWHM at 11 K, showing the correlation between N and static disorder. (d) Schematic illustrating how static disorder leads to an inhomogenously broadened lineshape and exciton localization.

N shows a good correlation with the inverse of the PL linewidth as shown in Fig. 4a, which implies that phonon scattering serves as the main mechanism for temperature-dependent decoherence (Fig. 4b). The temperature-dependence of N can be explained by exciton-phonon

scattering creating a nonuniform, temperature-dependent population distribution of energy levels in momentum space k.[18] At lower temperatures, only the $k = 0$ state is populated which corresponds to a coherence length extending over multiple QDs. Exciton-phonon scattering transfers oscillator strength from the $k = 0$ state to other momentum states at high temperatures.[18, 45] The spatial coherence length is restricted to a single QD as temperature increases above 100 K. In addition to phonon scattering, thermal averaging over superradiant and subradiant states could also reduce the coherence length and radiative rate at elevated temperatures.

Next, we discuss how static disorder and defects limit superradiance. SLs with narrower linewidth and lower static disorder showed faster radiative rates and a larger *N* (Fig. 4c). The relationship between exciton delocalization and static disorder is summarized in Fig. 4d. While SLs in samples A, C, D, and E all display a high radiative rate (1.5-3.2 ns^{-1}) and relatively narrow FWHM (< 25 meV) at 11 K, the radiative rate of the B SLs is much lower (0.2-0.8 ns^{-1}) with broader FWHM (33-36 meV), corresponding to *N* values smaller than 1 at 11 K. *N* less than 1 indicates that the emission is subradiant (i.e. the exciton is localized to a coherent spatial extension smaller than the exciton in isolated QDs), which is likely due to defect-induced localized states, for example from vacancies or dislocations in the lattices.[46] Fig. S16 shows that over a broad temperature range, *N* for the B1 SL remains near or less than 1, suggesting the emission is dominated by localized excitons.

For C, D, and E SLs, the overall behavior is similar to the A SLs but with lower *N* (1.5-2 at 11 K). Larger static disorder in the C and D SLs can localize exciton wavefunctions by introducing random phase shifts, resulting in a smaller *N*. Another factor is defect-induced localized states, which are likely to be more prevalent in C, D, and E SLs than in A SLs. As shown in Fig. S11, we observed a decrease in the relative PLQY for the C, D, and E SLs when the

temperature is below 50 K. We did not observe this behavior in SL A1 (Fig. 2c). This is likely due to some excitons being trapped in defect-induced localized states that lie below the superradiant bright state, which leads to a smaller *N*. We also compared results from a spun-cast film to that of the A1 SL (Fig. S17). The FWHM and experimental lifetime at low temperatures for the spun-cast film fall between the isolated QDs and the SL, due to aggregation likely occurring in the spun-cast film (Fig. S5c-d). Exciton superradiance is not limited to SLs with long-range order but should also be possible in thin films with short-range order so long as electron coupling can outcompete disorder, as demonstrated in recent works where red-shifted and increased exciton absorption was observed at low temperatures in QD thin films.[41, 47] Most recently, superfluorescence has also been reported in thin films of quasi two-dimensional $CsPbBr_3$.[48]

In conclusion, we reported the observation of superradiant decay from a delocalized exciton state with a coherence number of ~ 3 in SLs constructed from colloidal $CsPbBr_3$ QDs. Ultimately, *N* is determined by the competition between electronic coupling and disorder.[17, 18] The large oscillator strength leads to electronic coupling between QDs with energies of ~16 meV. For the more ordered SLs, the electronic coupling can outcompete both static and dynamic disorder at low temperatures, leading to an average *N* of 3. It is not surprising that QDs in highly inhomogeneous environments, such as in the B SLs (static disorder >30 meV), would be unable to establish superradiance, as the energetic disorder is too great to allow the delocalization of excitons. These results suggest that further enhancement of coherence length requires increasing electronic coupling through tuning QD size and ligand design as well as improving materials synthesis to decrease static disorder. The homogenous linewidth at zero temperature for a single $CsPbBr_3$ QD has been reported to be ~80 μeV,[32] much smaller than the Γ_0 at low temperature for the SLs here; thus, there is significant room to further reduce static disorder. For future studies, it

will also be desirable to directly correlate structural disorder to coherence by performing high-resolution TEM and temperature-dependent optical spectroscopy measurements on the same SL.

ASSOCIATED CONTENT

Supporting Information

The Supporting Information is available free of charge. Experimental details, including synthesis of QDs, SLs, isolated QD PMMA film and spun-cast film, steady-state and time resolved PL measurements; characterization of colloidal QD solutions, TEM and HAADF-STEM images of SLs; calculation of coupling strength, radiative rate and coherence number; supplemental figures (Figures S1-S17) including TEM of colloidal QDs, XRD spectrum, optical images of SLs, temperature-dependent PL and dynamics spectra of SLs and films, power-dependent dynamics spectra of a SL, temperature-dependent reflectance spectra of isolated QDs, PL intensity map of a SL; supplemental tables (Tables S1 and S2) for SLs' electron phonon coupling strength and colloidal QDs' optical properties and sizes.

AUTHOR INFORMATION

Corresponding Author

*E-mail: libai-huang@purdue.edu, christinawli@purdue.edu

Author Contributions

D.D.B., V.A.L., and D.E.C. contributed equally to this work.

Notes

The authors declare no competing financial interest.

ACKNOWLEDGMENTS

The work at Purdue is supported by the National Science Foundation through the Grant 2004339. The work was supported in part by the Research Instrumentation Center in the Department of Chemistry at Purdue University. Use of the Center for Nanoscale Materials, an Office of Science

user facility, was supported by the U. S. Department of Energy, Office of Science, Office of Basic Energy Sciences, under Contract No. DE-AC02-06CH11357.

REFERENCES

1. Dicke, R. H. Coherence in Spontaneous Radiation Processes. *Physical Review* 1954, *93*, 99-110.
2. Timothy Noe Ii, G.; Kim, J.-H.; Lee, J.; Wang, Y.; Wójcik, A. K.; McGill, S. A.; Reitze, D. H.; Belyanin, A. A.; Kono, J. Giant Superfluorescent Bursts from a Semiconductor Magneto-Plasma. *Nat Phys* 2012, *8*, 219-224.
3. Fidder, H.; Wiersma, D. A. Collective Optical Response of Molecular Aggregates. *physica status solidi (b)* 1995, *188*, 285-295.
4. Cong, K.; Zhang, Q.; Wang, Y.; Noe, G. T.; Belyanin, A.; Kono, J. Dicke Superradiance in Solids. *Journal of the Optical Society of America B* 2016, *33*, C80.
5. Rainò, G.; Nedelcu, G.; Protesescu, L.; Bodnarchuk, M. I.; Kovalenko, M. V.; Mahrt, R. F.; Stöferle, T. Single Cesium Lead Halide Perovskite Nanocrystals at Low Temperature: Fast Single-Photon Emission, Reduced Blinking, and Exciton Fine Structure. *ACS Nano* 2016, *10*, 2485-2490.
6. Jurow, M. J., et al. Manipulating the Transition Dipole Moment of Cspbbr3 Perovskite Nanocrystals for Superior Optical Properties. *Nano Lett* 2019, *19*, 2489-2496.
7. Koscher, B. A.; Swabeck, J. K.; Bronstein, N. D.; Alivisatos, A. P. Essentially Trap-Free Cspbbr3 Colloidal Nanocrystals by Postsynthetic Thiocyanate Surface Treatment. *J Amer Chem Soc* 2017, *139*, 6566-6569.
8. Liu, F., et al. Highly Luminescent Phase-Stable Cspbi3 Perovskite Quantum Dots Achieving near 100% Absolute Photoluminescence Quantum Yield. *ACS Nano* 2017, *11*, 10373-10383.
9. He, X.; Qiu, Y.; Yang, S. Fully-Inorganic Trihalide Perovskite Nanocrystals: A New Research Frontier of Optoelectronic Materials. *Adv Mater* 2017, *29*, 1700775.
10. Protesescu, L.; Yakunin, S.; Bodnarchuk, M. I.; Krieg, F.; Caputo, R.; Hendon, C. H.; Yang, R. X.; Walsh, A.; Kovalenko, M. V. Nanocrystals of Cesium Lead Halide Perovskites (Cspbx3, X = Cl, Br, and I): Novel Optoelectronic Materials Showing Bright Emission with Wide Color Gamut. *Nano Lett* 2015, *15*, 3692-3696.
11. Utzat, H., et al. Coherent Single-Photon Emission from Colloidal Lead Halide Perovskite Quantum Dots. *Science* 2019, *363*, 1068-1072.
12. Becker, M. A., et al. Bright Triplet Excitons in Caesium Lead Halide Perovskites. *Nature* 2018, *553*, 189-193.
13. Rainò, G.; Utzat, H.; Bawendi, M. G.; Kovalenko, M. V. Superradiant Emission from Self-Assembled Light Emitters: From Molecules to Quantum Dots. *MRS Bull* 2020, *45*, 841-848.
14. Rainò, G.; Becker, M. A.; Bodnarchuk, M. I.; Mahrt, R. F.; Kovalenko, M. V.; Stöferle, T. Superfluorescence from Lead Halide Perovskite Quantum Dot Superlattices. *Nature* 2018, *563*, 671-675.
15. Cherniukh, I., et al. Perovskite-Type Superlattices from Lead Halide Perovskite Nanocubes. *Nature* 2021, *593*, 535-542.
16. Röhlsberger, R.; Schlage, K.; Sahoo, B.; Couet, S.; Rüffer, R. Collective Lamb Shift in Single-Photon Superradiance. *Science* 2010, *328*, 1248-1251.

17. Spano, F. C.; Mukamel, S. Superradiance in Molecular Aggregates. *J Chem Phys* 1989, *91*, 683-700.
18. Spano, F. C.; Kuklinski, J. R.; Mukamel, S. Temperature-Dependent Superradiant Decay of Excitons in Small Aggregates. *Phys Rev Lett* 1990, *65*, 211-214.
19. Potma, E. O.; Wiersma, D. A. Exciton Superradiance in Aggregates: The Effect of Disorder, Higher Order Exciton-Phonon Coupling and Dimensionality. *J Chem Phys* 1998, *108*, 4894-4903.
20. Meinardi, F.; Cerminara, M.; Sassella, A.; Bonifacio, R.; Tubino, R. Superradiance in Molecular H Aggregates. *Phys Rev Lett* 2003, *91*, 247401.
21. Arias, D. H.; Stone, K. W.; Vlaming, S. M.; Walker, B. J.; Bawendi, M. G.; Silbey, R. J.; Bulović, V.; Nelson, K. A. Thermally-Limited Exciton Delocalization in Superradiant Molecular Aggregates. *J Phys Chem B* 2013, *117*, 4553-4559.
22. Doria, S., et al. Photochemical Control of Exciton Superradiance in Light-Harvesting Nanotubes. *ACS Nano* 2018, *12*, 4556-4564.
23. Krieg, F., et al. Monodisperse Long-Chain Sulfobetaine-Capped Cspbbr3 Nanocrystals and Their Superfluorescent Assemblies. *ACS Central Science* 2021, *7*, 135-144.
24. Coffey, B.; Friedberg, R. Effect of Short-Range Coulomb Interaction on Cooperative Spontaneous Emission. *PhRvA* 1978, *17*, 1033-1048.
25. Tepliakov, N. V.; Vovk, I. A.; Leonov, M. Y.; Baranov, A. V.; Fedorov, A. V.; Rukhlenko, I. D. Electronic and Optical Properties of Perovskite Quantum-Dot Dimer. *Semiconductors* 2019, *53*, 2158-2161.
26. Vovk, I. A.; Tepliakov, N. V.; Baimuratov, A. S.; Leonov, M. Y.; Baranov, A. V.; Fedorov, A. V.; Rukhlenko, I. D. Excitonic Phenomena in Perovskite Quantum-Dot Supercrystals. *Phys Chem Chem Phys* 2018, *20*, 25023-25030.
27. Cheng, O. H.-C.; Qiao, T.; Sheldon, M.; Son, D. H. Size- and Temperature-Dependent Photoluminescence Spectra of Strongly Confined Cspbbr $_3$ Quantum Dots. *Nanoscale* 2020, *12*, 13113-13118.
28. Chuang, C.; Cao, J. Universal Scalings in Two-Dimensional Anisotropic Dipolar Excitonic Systems. *Phys Rev Lett* 2021, *127*, 047402.
29. Yoon, S. J.; Guo, Z.; dos Santos Claro, P. C.; Shevchenko, E. V.; Huang, L. Direct Imaging of Long-Range Exciton Transport in Quantum Dot Superlattices by Ultrafast Microscopy. *ACS Nano* 2016, *10*, 7208-7215.
30. p't Hooft, G. W.; van der Poel, W. A. J. A.; Molenkamp, L. W.; Foxon, C. T. Giant Oscillator Strength of Free Excitons in Gaas. *Phys Rev B* 1987, *35*, 8281-8284.
31. Feldmann, J.; Peter, G.; Göbel, E. O.; Dawson, P.; Moore, K.; Foxon, C.; Elliott, R. J. Linewidth Dependence of Radiative Exciton Lifetimes in Quantum Wells. *Phys Rev Lett* 1987, *59*, 2337-2340.
32. Yu, B.; Zhang, C.; Chen, L.; Huang, X.; Qin, Z.; Wang, X.; Xiao, M. Exciton Linewidth Broadening Induced by Exciton–Phonon Interactions in Cspbbr3 Nanocrystals. *J Chem Phys* 2021, *154*, 214502.
33. Lee, J.; Koteles, E. S.; Vassell, M. Luminescence Linewidths of Excitons in Gaas Quantum Wells Below 150 K. *Phys Rev B* 1986, *33*, 5512.
34. Fivaz, R.; Mooser, E. Electron-Phonon Interaction in Semiconducting Layer Structures. *Physical Review* 1964, *136*, A833-A836.
35. Kaasbjerg, K.; Thygesen, K. S.; Jacobsen, K. W. Phonon-Limited Mobility Inn-Type Single-Layer Mos2from First Principles. *Phys Rev B* 2012, *85*, 115317.

36. Kim, S., et al. High-Mobility and Low-Power Thin-Film Transistors Based on Multilayer Mos2 Crystals. *Nat Commun* 2012, *3*, 1011.
37. Ramade, J., et al. Exciton-Phonon Coupling in a Cspbbr3 Single Nanocrystal. *Appl Phys Lett* 2018, *112*, 072104.
38. Fu, M.; Tamarat, P.; Trebbia, J.-B.; Bodnarchuk, M. I.; Kovalenko, M. V.; Even, J.; Lounis, B. Unraveling Exciton–Phonon Coupling in Individual Fapbi3 Nanocrystals Emitting near-Infrared Single Photons. *Nat Commun* 2018, *9*, 3318.
39. Mattiotti, F.; Kuno, M.; Borgonovi, F.; Jankó, B.; Celardo, G. L. Thermal Decoherence of Superradiance in Lead Halide Perovskite Nanocrystal Superlattices. *Nano Lett* 2020, *20*, 7382-7388.
40. Enomoto, K.; Oizumi, R.; Aizawa, N.; Chiba, T.; Pu, Y.-J. Energy Transfer from Blue-Emitting Cspbbr3 Perovskite Nanocrystals to Green-Emitting Cspbbr3 Perovskite Nanocrystals. *J Phys Chem C* 2021, *125*, 19368-19373.
41. Diroll, B. T.; Zhou, H.; Schaller, R. D. Low-Temperature Absorption, Photoluminescence, and Lifetime of Cspbx3 (X = Cl, Br, I) Nanocrystals. *Adv Funct Mater* 2018, *28*, 1800945.
42. Zhang, Z., et al. Ultrafast Exciton Transport at Early Times in Quantum Dot Solids. *Nat Mater* 2022, *21*, 533-539.
43. Lapkin, D., et al. Spatially Resolved Fluorescence of Caesium Lead Halide Perovskite Supercrystals Reveals Quasi-Atomic Behavior of Nanocrystals. *Nat Commun* 2022, *13*, 892.
44. Wei, K.; Zheng, X.; Cheng, X.; Shen, C.; Jiang, T. Observation of Ultrafast Exciton–Exciton Annihilation in Cspbbr3 Quantum Dots. *Advanced Optical Materials* 2016, *4*, 1993-1997.
45. Fidder, H.; Knoester, J.; Wiersma, D. A. Superradiant Emission and Optical Dephasing in J-Aggregates. *Chem Phys Lett* 1990, *171*, 529-536.
46. van der Burgt, J. S., et al. Cuboidal Supraparticles Self-Assembled from Cubic Cspbbr3 Perovskite Nanocrystals. *J Phys Chem C* 2018, *122*, 15706-15712.
47. Shcherbakov-Wu, W.; Sercel, P. C.; Krieg, F.; Kovalenko, M. V.; Tisdale, W. A. Temperature-Independent Dielectric Constant in Cspbbr3 Nanocrystals Revealed by Linear Absorption Spectroscopy. *J Phys Chem Lett* 2021, *12*, 8088-8095.
48. Biliroglu, M., et al. Room-Temperature Superfluorescence in Hybrid Perovskites and Its Origins. *Nat Photonics* 2022, *16*, 324-329.

TOC Graphic